

Laser cooling assisted thermal management of lightsails

Weiliang Jin,¹ Wei Li,^{1,2} Chinmay Khandekar,¹ Meir Orenstein,³ and Shanhui Fan¹

¹*Department of Electrical Engineering, Ginzton Laboratory, Stanford University, Stanford, California 94305, USA*

²*GPL Photonics Laboratory, State Key Laboratory of Applied Optics,
Changchun Institute of Optics, Fine Mechanics and Physics,
Chinese Academy of Sciences, Changchun 130033, China*

³*Department of Electrical Engineering, Technion-Israel Institute of Technology, 32000 Haifa, Israel*

A lightsail can be accelerated to relativistic speed by the radiation pressure of a laser having an intensity of the order of GW/m^2 . Such an extreme light intensity presents a critical challenge in the thermal management of lightsails. In this letter, we propose to use solid-state laser cooling for dissipating heat from such a lightsail. Our approach uses the same laser that is accelerating the sail, and can be used in addition to the previously explored radiative cooling. With our approach, we show that the cooling rate of a sail composed of a micron-thick layer doped with ytterbium ions can exceed that of blackbody thermal emission. This allows illumination by higher intensity lasers, and consequently shortens the acceleration distance to reach relativistic speed. Due to the Doppler shift, the performance of our approach is impacted by the limited bandwidth of the laser cooling dopant. When a constant-frequency pumping laser is used, laser cooling is particularly helpful for target velocities $\lesssim 0.05c$ for room-temperature operations.

Recent advances in high-power laser technology have stimulated progress in both fundamental physics and many applications relying on strong laser-matter interactions [1]. For instance, intense laser pulses have been explored to accelerate electrons [2, 3] and ions [4] to a relativistic speed. More recently, there is a growing interest in accelerating macroscopic objects to high speeds as well. Notable examples include fast-transit earth orbital maneuvering and interplanetary flight [5], and the Starshot Breakthrough Initiative that aims to accelerate a meter-size lightsail to 20% of the speed of light, so that it can reach a nearby star Proxima Centauri in 20 years [6, 7]. Many aspects of lightsail design have been discussed [8, 9], including efficient propulsion [9–11], thermal management [12], and self-stabilization [13–16].

A critical issue related to the necessary use of high-power laser for lightsail acceleration is the heat generated due to the residual optical absorption, even for a very low-loss dielectric sail, and the resultant heat that has to be dissipated efficiently to avoid material damage [17, 18]. This is exasperated by the fact that material absorption in general increases with temperature, causing significant thermal runaway [19]. The challenge is becoming more critical in space where heat cannot be dissipated through conduction or convection. Radiative cooling, which is based on thermal radiation, is thus the only approach explored for cooling a lightsail [8, 12]. In this context, simultaneous optimization for laser propulsion and thermal emission have been performed [20], but implementing the resulting photonic design over a meter-scale surface for emissivity enhancement remains challenging.

On the other hand, the same laser beam that causes heating might be exploited to provide cooling by applying the concept of solid-state laser cooling based on anti-Stokes fluorescence [21–23]. Laser cooling in solids has been successfully demonstrated in several materials including rare-earth ion doped fluoride glass, crystals [21, 23] and silica glass [24–26], and is extensively pursued in semiconductors [27–29]. One application of laser cooling is to provide solid-state re-

frigeration from room temperature to cryogenic temperatures, requiring the rare-earth ions to have near-unity quantum yield and the host media to be crystalline to enhance the absorption cross section of the ions [22]. A remarkable low temperature of 91 K has been experimentally achieved [30]. Another application is related to high-power lasers. The concept of radiation-balanced fiber lasers [18, 24, 31, 32] has been proposed to balance the heat generated by the Stokes-shifted lasing process with anti-Stokes fluorescence. The light intensity inside the fiber can be as high as $\sim \text{GW}/\text{m}^2$, approaching the value expected in the lightsail setups. Laser cooling operating at elevated temperature has also been discussed [33], where an improved cooling efficiency is to be expected.

In this article, we explore the possibility of adopting solid-state laser cooling based on rare-earth ions to address the thermal management challenge in the lightsail, which will potentially allow for more intense laser power and therefore shorter acceleration distance for the lightsail to reach the target velocity. Compared to prior laser cooling applications, there are at least three unique aspects in the lightsail platform: the operating temperature being higher than previously explored values; the laser intensity flux substantially saturating the absorption of the rare-earth ions; and the laser frequency experiencing significant Doppler redshift in the lightsail frame during the acceleration. The choice of the materials and the design of structures need to take these unique aspects into account. Here we develop a formalism for the design of laser-cooled lightsails. This formalism characterizes the performance of the laser cooling by the thermally constrained acceleration distance, with which the dual interplay between the optical and the thermal processes are captured. The minimization of acceleration distance is crucial for lowering both the power consumption and laser array size [12]. With our formalism, we show that laser cooling in micron-thick structures can offer substantial cooling power compared to blackbody emission, which leads to large improvement for the acceleration distance (potentially, up to $\gtrsim 20\times$ in the ideal regime, or $\gtrsim 10\times$

for the state-of-art). We explore the dependence on various parameters, including the material's absorption and the lightsail's temperature and target velocity. We find that laser cooling, in the simplest settings, is particularly relevant for lower temperatures and target velocities of few percents the speed of light. We finally study the possibility of having a variable laser intensity during the acceleration stage, which makes the most benefit of the laser cooling power and gives additional improvement for the acceleration distance.

I. THEORY

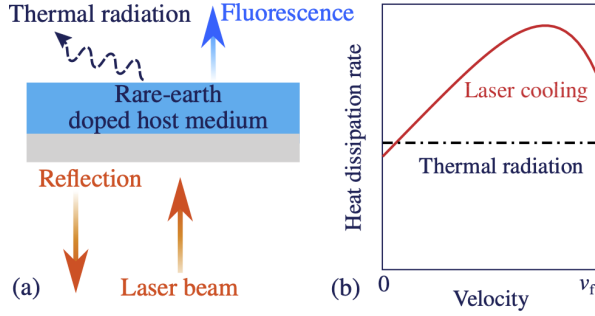


Figure 1: (a) Schematic of the concept of a laser-cooled lightsail. Most energy of the incident laser beam is reflected and contributes to the optical force for the propulsion, while some light power is parasitically absorbed and leads to heating. The heat is dissipated by thermal radiation, as well as via the anti-Stokes emission from the laser-excited rare-earth ions with fluorescence frequency higher than the incident laser frequency. (b) Schematic of total heat dissipation rate from the lightsail held at a constant temperature as a function of the velocity of the lightsail. All quantities are defined in the lightsail frame. The rate is constant for thermal radiation alone (black dotted-dashed curve), but exhibits variations with laser cooling (red solid curve) due to relativistic effects on the received laser intensity and Doppler-shifted frequency [12] that can alter laser cooling rate described by Eq. 4 in the main text.

As schematically illustrated in Fig. 1, a high-power laser beam is incident on a multi-layered lightsail, with at least one layer doped with rare-earth ions. The laser beam provides propulsion through radiation pressure, but nevertheless heats up the lightsail by its residual optical absorption. To balance against the heat generation, a portion of the laser light is used to pump the rare earth ions, which results in heat removal by anti-Stokes fluorescence on the top of the native thermal radiation. Below we briefly discuss formulations of the aforementioned processes, which are required to the study the acceleration and thermal balance of the lightsail.

The lightsail propulsion, as established in previous research [12, 34], depends crucially on the reflectivity that determines the momentum transfer, and the mass density that impacts the acceleration rate. A comprehensive figure of merit that captures the trade-off between the two is the distance D for the lightsail to be accelerated to a target velocity, described

by the following equation [9, 10, 35],

$$D = \frac{c^3}{2}(\rho_l + \rho_s) \int_0^{\beta_f} \frac{1}{I_p(\beta)} \frac{\gamma\beta d\beta}{R[\lambda_\beta](1-\beta)^2} \quad (1)$$

In Eq. 1, c is the speed of light, $\beta = v/c$ the velocity normalized by c , $\gamma = 1/\sqrt{1-\beta^2}$ the Lorentz factor, β_f the target velocity, ρ_s (ρ_l) the area mass density of the lightsail (payload), I_p the laser intensity averaged over the lightsail area when observed in the earth frame (where we explicitly included the β dependence for when the intensity is made variable during the acceleration stage). The reflectivity R , defined in the lightsail frame, is a function of the laser wavelength λ that experiences Doppler redshift from the laser wavelength in the rest frame λ_p as described by $\lambda_\beta = \lambda_p \sqrt{(1+\beta)/(1-\beta)}$.

Eq. 1 suggests that D can be decreased by simply boosting the laser intensity I_p . However, the optical power absorption of the lightsail also increases with I_p , which due to limited heat dissipation channels, can significantly raise the temperature of the lightsail. To avoid material damage, the highest temperature during the entire propulsion process [9, 12] must be below a threshold temperature T_s . Such a thermal management consideration imposes an upper limit on the allowed laser intensity, denoted $I_{p,\max}$. Other sources of material damage under high-power laser illumination such as plasma formation and ablation are typically reserved for short-pulses [36] and are not considered here. $I_{p,\max}$ can be found by considering the thermal balance in the co-moving frame of the lightsail,

$$I_{\text{abs}}(I_{\text{sail}}, \beta) \leq I_{\text{th}}(T_s) + I_{\text{cool}}(I_{\text{sail}}, T_s, \beta), \quad \forall \beta \in [0, \beta_f], \quad (2)$$

throughout the entire acceleration stage, where $I_{\text{sail}}(\beta) = I_p \frac{1-\beta}{1+\beta}$ is the laser intensity in the lightsail frame [12], and I_{abs} , I_{th} , and I_{ion} denote the power flows per unit area corresponding to optical absorption, thermal radiation, and laser cooling respectively. More explicitly, the absorbed power per unit area can be expressed as $I_{\text{abs}}(\beta) = I_{\text{sail}}(\beta)A(\lambda_\beta)$ that directly depends on $I_{\text{sail}}(\beta)$, and $A(\lambda_\beta)$, the absorptivity of the lightsail.

The computation of thermal radiation from a multilayer structure is well established, which can be expressed as [12]

$$I_{\text{th}}(T_s) = \int_0^\infty d\lambda \varepsilon(\lambda) \pi I_{\text{BB}}(\lambda, T_s) \quad (3)$$

where $\varepsilon(\lambda)$ is the hemispherical-spectral emissivity summing over the front and back surface, and $I_{\text{BB}}(\lambda, T_s) = \frac{2hc^2}{\lambda^5} \left[\exp\left(\frac{hc}{\lambda k_B T_s}\right) - 1 \right]^{-1}$ the blackbody spectral intensity.

Finally, we compute $I_{\text{cool}}(I_{\text{sail}}, T_s, \beta)$ using the recently developed adaptive four-level model [37] that captures the main features of laser cooling operating at elevated temperatures. This simple phenomenological model, validated against experimental results, can accurately predict the cooling performance over a wide range of temperatures and pumping frequencies using only a small number of parameters that can

be determined from experiments. This is particularly relevant to the lightsail problem since the pumping wavelength can undergo significant Doppler shift [Fig. 1(b)]. The rare-earth ions, responsible for the laser cooling, absorb light over a narrow frequency range since the bandwidths of the excited and ground states manifold that contribute to the absorption are relatively narrow. The laser cooling rate is

$$P_{\text{cool}}(I, T_s, \omega_p) = \left[\eta_e \frac{\omega_f}{\omega_p} - 1 \right] \alpha(I, T_s, \omega_p) I \quad (4)$$

where η_e is the external quantum yield and $\alpha(I, T_s, \omega_p)$ is the absorption coefficient of the ions that depends on the pumping frequency ω_p and the local light intensity I at the position of ions, as follows,

$$\alpha(I) = \frac{\alpha_0}{1 + I/I_s}, \quad \text{with} \quad \alpha_0 = \frac{\sigma_{12} N_t}{1 + \exp[\hbar\Delta/k_B T_s]}. \quad (5)$$

σ_{12} is the atomic absorption cross section for the transition from the top of the ground manifold to the bottom of the excited manifold, N_t the doping concentration, $I_s = \hbar\omega\gamma/\sigma_{12}$ the saturation intensity. Δ is the effective manifold width, which is a solution of the following equation, assuming a given mean fluorescence frequency ω_f ,

$$\omega_f = \omega_p + \Delta \left[\frac{1}{2} + \frac{1}{1 + \exp[\hbar\Delta/k_B T_s]} \right]. \quad (6)$$

Neglecting fluorescence reabsorption [38], the net cooling power I_{cool} needed in Eq. 2 can then be computed simply by integrating P_{cool} over the layer thickness t , which gives an increasing I_{cool} with thickness. This is the relevant regime for thin lightsails where only a small fraction of the incident light is absorbed. Finally, note that in laser cooling setups, there is an additional parasitic absorption term $\alpha_b I$ which is not included in Eq. 4, but is directly accounted for in the optical absorption I_{abs} in Eq. 2. This parasitic absorption contributes to heating, while the absorption α in Eq. 4 leads to cooling.

We note that Eq. 4 can be simplified in the high intensity regime, which is relevant for lightsail platforms where the typical laser intensity ($I_p \gtrsim 10 \text{ GW/m}^2$ [6, 9]) is far above the saturation intensity ($I_s \approx 0.1 \text{ GW/m}^2$ [24] for typical parameters of rare-earth ions, including $\gamma \approx 10^3 \text{ s}^{-1}$ [39] and $\sigma_{12} \approx 10^{-20} \text{ cm}^{-2}$ [24]). In this limit, the cooling power density yields a simpler expression,

$$P_{\text{cool}} = \left(\eta_e \frac{\omega_f}{\omega_p} - 1 \right) \frac{N_t \hbar \omega_p \gamma}{1 + \exp[\hbar\Delta/k_B T_s]} \quad (7)$$

Therefore, P_{cool} depends linearly on the decay rate γ and the doping concentration N_t , but is independent on the light intensity I . P_{cool} is also independent of σ_{12} , which is very different from laser cooling applications pursuing cryogenic refrigeration whose performances can be greatly improved by enhancing σ_{12} [21]. In the ideal scenarios where $\eta_e \approx 1$, the peak cooling power density can be found by solving for ω_p

that maximizes Eq. 7,

$$P_{\text{cool},m} \approx 0.21 \gamma k_B T_s N_t$$

$$I_{\text{cool},m} \approx 0.21 \gamma k_B T_s N_t t, \quad \text{at} \quad \omega_p \approx \omega_f - 0.78 \frac{k_B T_s}{\hbar}, \quad (8)$$

where the corresponding relative bandwidth of the cooling spectrum, characterized by normalized full width at half maximum, is $1.24 \frac{k_B T_s}{\hbar \omega_p}$. This finite bandwidth can limit the laser cooling performance of a lightsail, as we explore later [Fig. 1(b)].

II. RESULTS

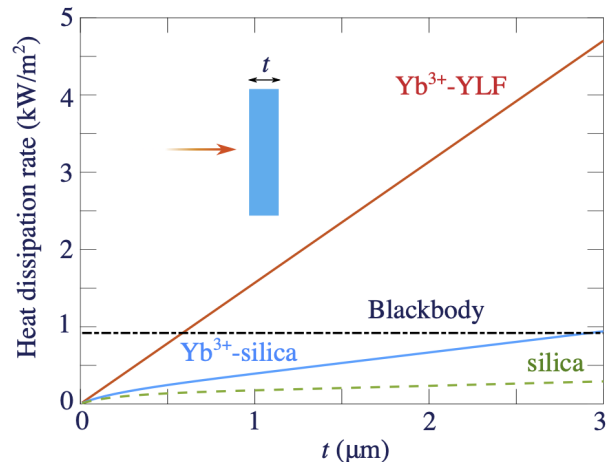


Figure 2: Heat dissipation rate per unit area at room temperature for ideal Yb^{3+} -doped YLF (red solid line) and Yb^{3+} -doped silica (blue solid line) in the saturated absorption regime where the laser intensity is far above the saturation intensity throughout the slab, compared to the heat dissipation rate due to blackbody emission (black dashed line) and thermal emission alone from silica slab (green dashed line). Note that the blue solid curve is for the summed contribution from thermal radiation and laser cooling. The doping level is assumed to be $1.4 \times 10^{21} \text{ cm}^{-3}$ for YLF [30] and $1.93 \times 10^{20} \text{ cm}^{-3}$ for silica [40], and the radiative lifetime is $\tau = 0.765 \text{ ms}$ [40].

In order to study the relevance of laser cooling in a lightsail, we first examine a simple single-slab geometry and compute heat dissipation rates due to thermal radiation and laser cooling for different materials (Fig. 2). We find that in the saturated regime (Eq. 8), laser cooling (solid lines) can substantially improve the heat dissipation rate compared to thermal radiation alone (dashed lines). In particular, due to laser cooling, a Yb^{3+} -doped silica slab (blue line) has a larger heat dissipation rate compared to an undoped layer that only relies on thermal radiation (dashed line). The heat dissipation rate is more than doubled for a $3 \mu\text{m}$ -thick layer assuming state-of-art doping level (indicated in the caption). However, even with the increase due to laser cooling, the total heat dissipation rate may still be considered relatively moderate for the lightsail application. On the other hand, a significantly larger heat dissipation rate is observed for a Yb^{3+} -doped LiYF_4 (YLF) layer

(red line) in the optimal laser cooling regime with a state-of-art doping level. With this material, the total dissipation rate can significantly exceed blackbody emission (dot-dashed line) using a micron-thick layer. This promising result suggests a large potential of improved thermal management in lightsails using laser cooling.

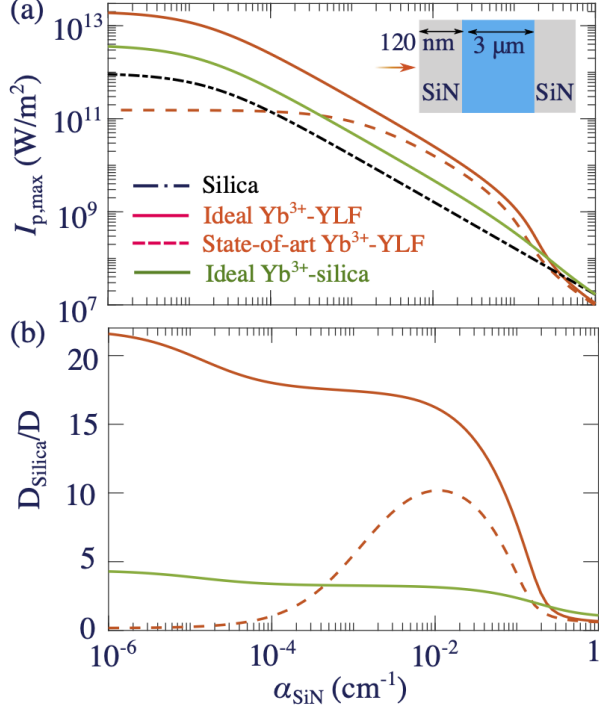


Figure 3: The maximum allowed pumping intensity (a) and improvement of the acceleration distance (b) using laser cooling (where the middle layer is either Yb³⁺-doped silica [green line] or Yb³⁺-doped YLF crystal [red curve]) compared to using undoped silica layer as a middle layer. We assume constant laser intensity during the acceleration stage. “Ideal” laser-cooled layer corresponds to $\eta_e = 100\%$ and $\alpha_b = \alpha_{\text{silica}} = 10^{-6} \text{ cm}^{-1}$ (we take a non-zero background absorption for fair comparison with undoped silica). We use the state-of-art parameters for Yb³⁺-YLF ($\eta_e = 99.6\%$, $\alpha_b = 10^{-4} \text{ cm}^{-1}$, radiative lifetime $\tau = 0.765 \text{ ms}$, $\sigma_{12} = 2.8 \times 10^{-21} \text{ cm}^{-2}$) and only consider the ideal case for Yb³⁺-silica (state-of-art gives relatively poor performance). The doping level is assumed to be the state-of-art in silica $1.93 \times 10^{20} \text{ cm}^{-3}$ [40] and YLF $1.4 \times 10^{21} \text{ cm}^{-3}$ [30]. Thermal radiation from both SiN and silica layers are considered.

In order to study more carefully the advantages of a lightsail application, we compute the resulting effects on the acceleration distance (Eq. 1). While both doped YLF and silica show potential promise for thermal management, their low refractive index gives small reflectivity, and thus small acceleration force. So, for lightsail applications, we need to combine the laser-cooling layer with other high-index materials [12]. As a representative example, we consider a trilayer structure depicted in the inset of Fig. 3, with the aim to achieve sufficient reflection as well as substantial cooling. The thickness of the two SiN layers at the edges is chosen as small as possible while still maximizing reflection for wavelengths around

$1 \mu\text{m}$. The middle layer is either silica or doped YLF and is used for thermal management. In all computations, we assume a configuration of a typical sail area of 10 m^2 and a payload mass of 1 kg . This configuration, where the mass of the micron-thick sail is relatively small compared to the kg-level payload, is adequate to reach a target velocity of few percents the speed of light with a laser intensity of the order of few GW/m^2 which corresponds to a Starshot-level beam [6, 7]. In order to quantify this, we compute the maximum lasing power $I_{p,max}$ and the corresponding acceleration distance D required to reach a target velocity of $0.01c$ (Fig. 3). Here we do not assume a particular form of the SiN absorption coefficient α_{SiN} as it highly depends on many processing-dependent factors [12]. Instead, we assess the performance of the lightsail at various values of α_{SiN} . We also assume a fixed small absorption for silica [12] ($\alpha_{\text{silica}} = 10^{-6} \text{ cm}^{-1}$) and Yb³⁺-doped YLF ($\alpha_b = 10^{-4} \text{ cm}^{-1}$ for the state-of-art [30] and $\alpha_b = \alpha_{\text{silica}}$ for the ideal case) in the middle layer. The specific choice of a threshold temperature T_s depends on the required operating conditions and the temperature dependence of the material properties [9]. As a reference, we now assume $T_s = 300 \text{ K}$ (and later explore the effects of changing T_s). The corresponding maximum allowed laser power $I_{p,max}$ is then computed by Eq. 2. For each configuration, we fine-tune the operating wavelength around $1 \mu\text{m}$ to minimize the acceleration distance D .

The results of the computation are shown in Fig. 3. In Fig. 3(b), we see that substantial reduction of the acceleration distance D is possible when using laser cooling, compared to using an undoped silica layer that only relies on thermal radiation. As shown in Fig. 3(a), this is due to the fact that laser cooling allows the use of higher beam intensities without exceeding the threshold temperature T_s . Note that, as expected, this maximum intensity $I_{p,max}$ always increases with decreasing absorption coefficient α_{SiN} , and saturates when the loss becomes dominated by the middle layer. Fig. 3(b) shows that, when using an ideal Yb³⁺-doped YLF layer (red solid curve), D can be decreased by large factors over a wide range of α_{SiN} values, reaching a maximum enhancement $D_{\text{silica}}/D \approx 22$ for small loss. For a state-of-art Yb³⁺-YLF layer (red dashed line), the larger parasitic absorption α_b of the middle layer limits the enhancement at small α_{SiN} values, since optical absorption becomes quickly dominated by the middle layer. Still, a large ($\approx 10\times$) decrease of D can be observed for intermediate absorption coefficient values. Finally, Yb³⁺-doped silica (solid green line) gives smaller improvement of at best a factor of ≈ 4 . The smaller improvement is expected and is due to the corresponding smaller heat dissipation rate, as already noted from the results of Fig. 2.

We further study the effects of changing the target velocity and the threshold damage temperature T_s when using a Yb³⁺-YLF layer in the optimal regime of laser cooling [Fig. 4(a,b)-dashed lines]. As expected, the acceleration-distance enhancement D_{silica}/D worsens with increasing target velocity since the operation bandwidth increases. In fact, because of Doppler shift, the operating wavelength substantially shifts

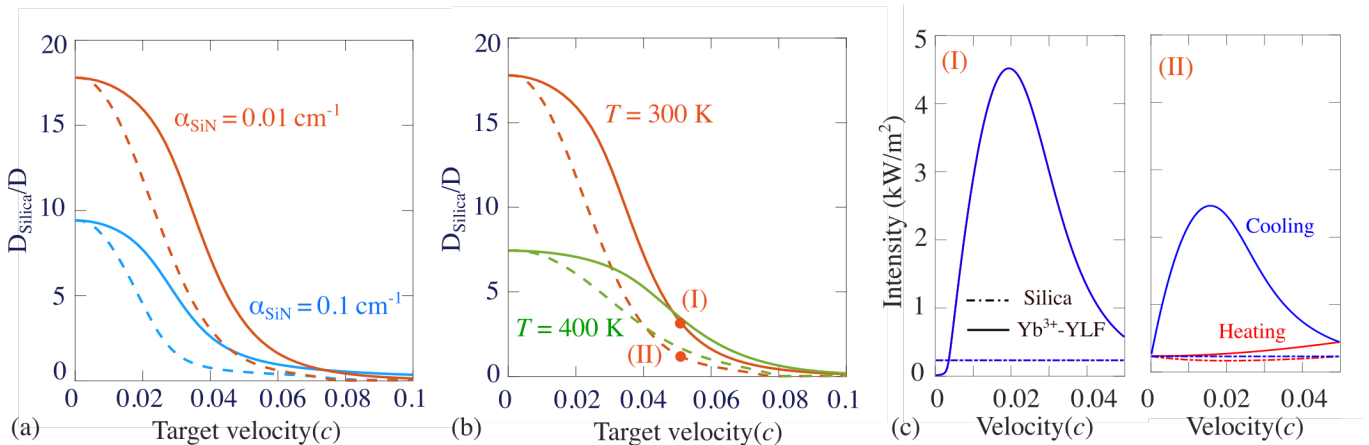


Figure 4: Results for the triple-layer setup shown in Fig. 3(a) using a Yb^{3+} doped YLF layer with small parasitic absorption ($\alpha_b = 10^{-6} \text{ cm}^{-1}$) and ideal quantum yield ($\eta_e = 100\%$). In (a,b), solid (resp. dashed) lines stand for tunable (resp. fixed) laser intensity during the acceleration stage. (a) Improvement of acceleration distance as a function of target velocity for different SiN absorption coefficients and an operating temperature $T_s = 300 \text{ K}$. (b) Improvement of acceleration distance at different operating temperatures and a given SiN absorption $\alpha_{\text{SiN}} = 10^{-2} \text{ cm}^{-1}$. (c) Heating/cooling intensity during the acceleration process for target velocity $0.05c$ [red dots in (b)] corresponding to tunable (I) and fixed (II) laser intensity, using a laser-cooler Yb^{3+} -YLF layer (solid) or radiatively-cooled silica layer (dashed). Note that for tunable laser intensity (I), heating and cooling curves are identical.

when the lightsail reaches high velocities and can get outside the laser cooling bandwidth. Fig. 4(a) [dashed lines] shows that D increases and becomes larger than the acceleration distance D_{silica} (corresponding to undoped silica) for target velocities nearing 10% of the speed of light. This effect is more pronounced for larger absorption coefficients. Similarly, Fig. 4(b) [dashed lines] reveals that laser cooling can play a more significant role when aiming at a lower threshold temperature due to the different temperature dependence for each heat dissipation mechanism, where the laser cooling scales as $\propto T_s$ from Eq. 8 and the thermal radiation as $\propto T_s^4$.

It is important to notice that, as the operating wavelength is Doppler shifted during the acceleration phase, the laser cooling power changes [e.g., Fig. 1(b)], meaning that the maximum laser intensity allowed for the structure to stay at below the threshold temperature T_s also varies. For example, for velocities where the laser cooling power is maximum, a larger laser intensity can be used without exceeding the temperature T_s . If the operating laser intensity is kept constant in the earth frame as the lightsail accelerates, then it has to match the value of $I_{p,\text{max}}$ corresponding to the lowest laser cooling power of the whole acceleration stage. So, in order to estimate the benefits of a variable laser intensity, we compute the corresponding enhancement in the acceleration distance D , as plotted in Fig. 4(a,b) [solid lines]. We see that noticeable improvement can be achieved, both as a function of the target velocity and the threshold temperature. To highlight this, we investigate the evolution of the cooling power during the acceleration stage in multiple settings, for a target velocity of $0.05c$. When the laser intensity is allowed to vary [Fig. 4(c,I)], heating and cooling intensities are exactly balanced during the whole acceleration stage. On the other hand, for a fixed laser intensity [Fig. 4(c,II)], exact balance occurs only at specific

velocities (here, 0 and $0.05c$). During most of the acceleration stage, the lightsail sees a net cooling at the threshold temperature T_s , meaning that its equilibrium temperature is strictly less than T_s . This allows for the laser intensity to be further increased during most of the acceleration stage without exceeding the threshold temperature T_s . It is this effect that is being exploited in a variable laser intensity setting, which allows for an overall decrease of the total acceleration distance D .

III. CONCLUSION

We have presented a general study for the prospect of using laser cooling as a thermal management tool in relativistic lightsails. Our results show the prospects of such method and the regime in which it is most relevant (micron-thick structures, few percents the speed of light, lower operating temperature, and appropriate absorption interval). When aiming for even higher target velocity where the limited operating bandwidth of laser cooling dopant to account for Doppler shift becomes the main challenge, one can potentially still harness laser cooling by using a laser of variable frequency, or using a few rare earth ion to span a wide operating bandwidth. Additionally, future work can focus on further design schemes to improve the potential of using laser cooling in a lightsail setting.

Acknowledgments W. Jin would like to thank Dr. Mohammed Benzaouia and Dr. Alex Song for useful contributions. This work is supported by the Breakthrough Starshot Initiative (initial idea and performance testing), and the U.S. Department of Energy “Photonics at Thermodynamic Limits” Energy Frontier Research Center under Grant No. DE-

SC0019140 (theoretical modeling).

-
- [1] Y. I. Salamin, S. Hu, K. Z. Hatsagortsyan, and C. H. Keitel, *Physics Reports* **427**, 41 (2006).
- [2] G. Malka, E. Lefebvre, and J. Miquel, *Physical Review Letters* **78**, 3314 (1997).
- [3] K. P. Wootton, Z. Wu, B. M. Cowan, A. Hanuka, I. V. Makasyuk, E. A. Peralta, K. Soong, R. L. Byer, and R. J. England, *Optics Letters* **41**, 2696 (2016).
- [4] T. Esirkepov, M. Borghesi, S. Bulanov, G. Mourou, and T. Tajima, *Physical Review Letters* **92**, 175003 (2004).
- [5] H.-T. Tung and A. R. Davoyan, *Nano Letters* **22**, 1108 (2022).
- [6] P. Lubin, arXiv preprint arXiv:1604.01356 (2016).
- [7] K. L. Parkin, *Acta Astronautica* **152**, 370 (2018).
- [8] M. M. Salary and H. Mosallaei, *Laser & Photonics Reviews* **14**, 1900311 (2020).
- [9] H. A. Atwater, A. R. Davoyan, O. Ilic, D. Jariwala, M. C. Sherrott, C. M. Went, W. S. Whitney, and J. Wong, *Nature Materials* **17**, 861 (2018).
- [10] W. Jin, W. Li, M. Orenstein, and S. Fan, *ACS Photonics* **7**, 2350 (2020).
- [11] Z. A. Kudyshev, A. V. Kildishev, V. M. Shalaev, and A. Boltasheva, *ACS Photonics* **9**, 190 (2021).
- [12] O. Ilic, C. M. Went, and H. A. Atwater, *Nano Letters* **18**, 5583 (2018).
- [13] O. Ilic and H. A. Atwater, *Nature Photonics* **13**, 289 (2019).
- [14] J. Siegel, A. Y. Wang, S. G. Menabde, M. A. Kats, M. S. Jang, and V. W. Brar, *ACS Photonics* **6**, 2032 (2019).
- [15] Z. Manchester and A. Loeb, *The Astrophysical Journal Letters* **837**, L20 (2017).
- [16] K. V. Myilswamy, A. Krishnan, and M. L. Povinelli, *Optics Express* **28**, 8223 (2020).
- [17] X. Liu, M. H. Hu, C. G. Caneau, R. Bhat, and C.-E. Zah, *IEEE Transactions on Components and Packaging Technologies* **29**, 268 (2006).
- [18] S. R. Bowman, *IEEE Journal of Quantum Electronics* **35**, 115 (1999).
- [19] G. R. Holdman, G. R. Jaffe, M. S. Jang, D. Feng, M. A. Kats, and V. W. Brar, arXiv preprint arXiv:2110.06185 (2021).
- [20] J. Brewer, M. F. Campbell, P. Kumar, S. Kulkarni, D. Jariwala, I. Bargatin, and A. P. Raman, *Nano Letters* **22**, 594 (2022).
- [21] D. V. Seletskiy, M. P. Hehlen, R. I. Epstein, and M. Sheik-Bahae, *Advances in Optics and Photonics* **4**, 78 (2012).
- [22] G. Nemova and R. Kashyap, in *Journal of Physics: conference series* (Institute of Physics and IOP Publishing Limited, 2015), vol. 619, p. 012037.
- [23] D. V. Seletskiy, R. Epstein, and M. Sheik-Bahae, *Reports on Progress in Physics* **79**, 096401 (2016).
- [24] J. Knall, P.-B. Vigneron, M. Engholm, P. D. Dragic, N. Yu, J. Ballato, M. Bernier, and M. J. Dignonnet, *Optics Letters* **45**, 1092 (2020).
- [25] E. Mobini, S. Rostami, M. Peysokhan, A. Albrecht, S. Kuhn, S. Hein, C. Hupel, J. Nold, N. Haarlammert, T. Schreiber, et al., *Communications Physics* **3**, 134 (2020).
- [26] M. Peysokhan, S. Rostami, E. Mobini, A. R. Albrecht, S. Kuhn, S. Hein, C. Hupel, J. Nold, N. Haarlammert, T. Schreiber, et al., arXiv preprint arXiv:2011.11224 (2020).
- [27] D. Huang, T. Apostolova, P. Alsing, and D. Cardimona, *Physical Review B* **70**, 033203 (2004).
- [28] S. Zhang, M. Zhukovskiy, B. Jankó, and M. Kuno, *NPG Asia Materials* **11**, 1 (2019).
- [29] M. Sheik-Bahae and R. I. Epstein, *Laser & Photonics Reviews* **3**, 67 (2009).
- [30] S. D. Melgaard, A. R. Albrecht, M. P. Hehlen, and M. Sheik-Bahae, *Scientific Reports* **6**, 20380 (2016).
- [31] J. M. Knall, M. Esmaelpour, and M. J. Dignonnet, *Journal of Lightwave Technology* **36**, 4752 (2018).
- [32] E. Balliu, A. Thontakudi, J. M. Knall, and M. J. Dignonnet, in *Photonic Heat Engines: Science and Applications* (International Society for Optics and Photonics, 2019), vol. 10936, p. 109360J.
- [33] Y. Nakayama, Y. Harada, and T. Kita, *Optics Express* **27**, 34961 (2019).
- [34] J. Chen, J. Ng, Z. Lin, and C. Chan, *Nature Photonics* **5**, 531 (2011).
- [35] N. Kulkarni, P. Lubin, and Q. Zhang, *The Astronomical Journal* **155**, 155 (2018).
- [36] B. Stuart, M. Feit, A. Rubenchik, B. Shore, and M. Perry, *Physical Review Letters* **74**, 2248 (1995).
- [37] W. Jin, C. Guo, M. Orenstein, and S. Fan, *Applied Physics Letters* **119**, 181107 (2021).
- [38] B. Heeg, P. A. DeBarber, and G. Rumbles, *Applied Optics* **44**, 3117 (2005).
- [39] M. J. Dignonnet, *Rare-earth-doped fiber lasers and amplifiers, revised and expanded* (CRC press, 2001).
- [40] J. M. Knall, M. Engholm, T. Boilard, M. Bernier, and M. J. F. Dignonnet, *Physical Review Letters* **127**, 013903 (2021).